

Interaction of Giant Unilamellar Vesicles with the Surface Nanostructures on Dragonfly Wings

Samuel Cheeseman,[†] Vi Khanh Truong,^{†,‡} Vivien Walter,[§] Fabrice Thalmann,[§] Carlos M. Marques,[§] Eric Hanssen,^{||} Jitraporn Vongsvivut,[⊥] Mark J. Tobin,[⊥] Vladimir A. Baulin,[#] Saulius Juodkazis,^{||} Shane Maclaughlin,^{‡,∇} Gary Bryant,[†] Russell J. Crawford,[†] and Elena P. Ivanova^{*,‡,†}

[†]School of Science, College of Science, Engineering and Health, RMIT University, GPO Box 2476, Melbourne, Victoria 3001, Australia

[‡]ARC Research Hub for Australian Steel Manufacturing, Wollongong, New South Wales 2522, Australia

[§]Université de Strasbourg, CNRS, Institut Charles Sadron, UPR022, 23 rue du Loess, 67034 Strasbourg Cedex, France

^{||}Advanced Microscopy Facility, Bio21 Institute, University of Melbourne, 30 Flemington Rd, Parkville, Victoria 3010, Australia

[⊥]Infrared Microspectroscopy Beamline, Australian Synchrotron, 800 Blackburn Road, Clayton, Victoria 3168, Australia

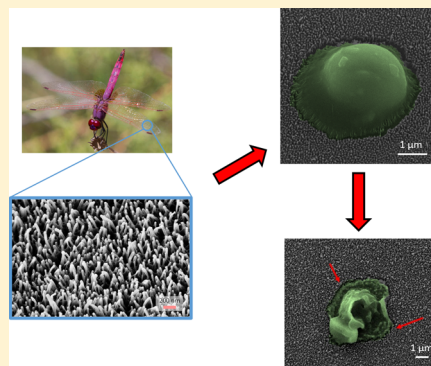
[#]Departament d'Enginyeria Quimica, Universitat Rovira, Virgili, 26 Av. dels Paisos Catalans, 43007 Tarragona, Spain

^{||}Centre for Micro-Photonics and Industrial Research Institute Swinburne, Faculty of Science, Engineering and Technology, Swinburne University of Technology, P.O. Box 218, Hawthorn, Victoria 3122, Australia

[∇]BlueScope Steel Research, Port Kembla, New South Wales 2505, Australia

Supporting Information

ABSTRACT: The waxy epicuticle of dragonfly wings contains a unique nanostructured pattern that exhibits bactericidal properties. In light of emerging concerns of antibiotic resistance, these mechano-bactericidal surfaces represent a particularly novel solution by which bacterial colonization and the formation of biofilms on biomedical devices can be prevented. Pathogenic bacterial biofilms on medical implant surfaces cause a significant number of human deaths every year. The proposed mechanism of bactericidal activity is through mechanical cell rupture; however, this is not yet well understood and has not been well characterized. In this study, we used giant unilamellar vesicles (GUVs) as a simplified cell membrane model to investigate the nature of their interaction with the surface of the wings of two dragonfly species, *Austrothemis nigrescens* and *Trithemis annulata*, sourced from Victoria, Australia, and the Baix Ebre and Terra Alta regions of Catalonia, Spain. Confocal laser scanning microscopy and cryo-scanning electron microscopy techniques were used to visualize the interactions between the GUVs and the wing surfaces. When exposed to both natural and gold-coated wing surfaces, the GUVs were adsorbed on the surface, exhibiting significant deformation, in the process of membrane rupture. Differences between the tensile rupture limit of GUVs composed of 1,2-dioleoyl-*sn*-glycero-3-phosphocholine and the isotropic tension generated from the internal osmotic pressure were used to indirectly determine the membrane tensions, generated by the nanostructures present on the wing surfaces. These were estimated as being in excess of 6.8 mN m^{-1} , the first experimental estimate of such mechano-bactericidal surfaces. This simple model provides a convenient bottom-up approach toward understanding and characterizing the bactericidal properties of nanostructured surfaces.



INTRODUCTION

The waxy epicuticular layer of the wing membranes of dragonflies possesses high-aspect-ratio nanoscale pillars, which are composed of lipids.^{1,2} Recently, it was discovered that these natural surface features could exhibit strong bactericidal behavior against Gram-positive, Gram-negative, and even spore-forming bacteria.^{2–4} This bactericidal activity has been successfully extended to synthetic analogues of the wings, which possess similar high-aspect-ratio nanoscale features.^{3,5–7} These surfaces present a unique solution to the rapidly growing problem of bacterial adhesion, proliferation,

and biofilm formation on orthopedic implants. These biofilms can cause fatalities placing a significant financial strain on the healthcare industry.^{8,9} In the USA alone, 17 million new biofilm infections occur annually and such infections are responsible for over half a million fatalities each year.¹⁰ It is currently believed that the bactericidal mechanism by which these nanostructured surfaces kill the bacteria is via a

Received: October 16, 2018

Revised: December 19, 2018

Published: January 10, 2019

mechanical rupture process. It is proposed that cells strongly adsorb onto the surface of the high-aspect-ratio surface nanofeatures, which causes the cell membrane to stretch between adjacent pillars, eventually causing them to rupture.¹¹ It has, however, been technically challenging to accurately characterize the interactions taking place between the surface of the bacterial cells and the nanoscale features of the substrate. This is because the bacterial cells are very small and the cell walls are highly complex, making it difficult to attain accurate measurements of their rigidity.¹² In addition, the nature of this interaction is complicated, involving short- and long-range physico-chemical forces, influenced by various aspects of the nanoscale structures and biological cells involved.¹³

Giant unilamellar vesicles (GUVs) are simple, synthetically produced spheres, consisting of a thin unilamellar membrane that encloses a given solution.^{14–16} GUVs can range from 1 to 150 μm in diameter.^{14–19} Unilamellar vesicles have been used for studying cellular protein activity, drug delivery systems, and the biophysical properties of membranes.^{20–23} GUVs can be well defined, with highly controllable features such as membrane composition, rigidity, internal contents, and turgor pressure.^{24,25} Their large size, simplicity, and adaptable composition make them suitable for application as an adjustable model of a bacterial cell membrane, allowing an analysis of each of the individual membrane components in isolation.²⁶

In this study, GUVs were utilized as a simplified model of the cell membrane in order to investigate the interactions taking place between the membrane and the mechano-bactericidal nanostructured surface of *Austrothemis nigrescens* and *Trithemis annulata* dragonfly wings. By constructing the GUV membrane using 1,2-dioleoyl-*sn*-glycero-3-phosphocholine (DOPC), with known biophysical properties, we were able to establish the range of stretching forces that can be imparted on the membrane by the nanofeatures that present on the dragonfly wings and thus infer the range of the tensions that are imposed on the cell membrane models by the dragonfly wings. This work provides a new insight into the optimal design of synthetic nanostructured surfaces with bactericidal activity, which can be useful for industrial and biomedical applications.

■ EXPERIMENTAL SECTION

Materials. The lipids were purchased from Avanti Polar Lipids (Alabaster, AL), dissolved in 5 mL of chloroform to form a lipid concentration of 1 mg/mL. These solutions were stored at $-20\text{ }^{\circ}\text{C}$ until needed. DOPC containing a 1% molar ratio of fluorescently labeled Liss Rhod PE (1,2-dipalmitoyl-*sn*-glycero-3-phosphoethanolamine-*N*-(lissamine rhodamine B sulfonyl)), which fluoresces red, was used to construct the GUVs. Both phospholipids exhibited an overall neutral charge. Fluorescein isothiocyanate (FITC) dextran, with an average molecular weight of 150 000, was purchased from Sigma-Aldrich (St. Louis, MO).

Dragonfly Collection and Sample Preparation. The dragonfly *A. nigrescens* and *T. annulata* specimens were collected in Victoria, Australia, and the Baix Ebre and Terra Alta regions of Catalonia, Spain, respectively. The wings were aseptically removed from the body and stored in dark conditions at room temperature (ca. $22\text{ }^{\circ}\text{C}$) in sterile polystyrene Petri dishes, purchased from Techno Plas (St Marys, Australia), until required. The distal-posterior regions of the forewings were dissected into approximately $5 \times 5\text{ mm}^2$ sections using a sterile surgical blade.

Scanning Electron Microscopy. The wing samples were coated with 7.5 nm gold films, according to the manufacturers' instructions, using a JEOL NeoCoater (JEOL Inc., Peabody, MA). High-resolution

scanning electron micrographs were obtained at 3 kV under 20 000 \times , 40 000 \times , and 70 000 \times magnification using a ZEISS SUPRA 40VP field emission scanning electron microscope (Carl Zeiss NTS GmbH, Oberkochen, Germany).

The scanning electron micrographs were analyzed using ImageJ software (version 1.50i). The color threshold for binary SEM images was adjusted, and the particles were analyzed. Particles with a diameter below 30 nm, smaller than the thinnest nanopillars, were removed from consideration as artefacts. For each dragonfly wing, the density of nanofeatures, inclusive of free-standing and clustered nanopillars, was determined using a particle analysis procedure, with measurements taken over six regions, $1.5\text{ }\mu\text{m} \times 2\text{ }\mu\text{m}$ in area, on each of the dragonfly wing surfaces. The diameter of free-standing nanopillars was manually measured using ImageJ because an automated approach was found to be unsuitable because of the natural bending and clustering of the nanopillars. Avizo software (version 7.0) was used to create three-dimensional images representative of the wing surfaces. Cross-sectional profiles were achieved by submerging both the natural and gold-coated wings in liquid nitrogen, then fracturing them prior to them being viewed using SEM. The height of the free-standing nanopillars was determined by tilting the samples at a 45° angle, with images being obtained using the high-resolution SEM capabilities of the electron beam lithography tool (Raith150 Two, Raith GmbH, Dortmund, Germany) at 5 kV. Measurements were performed using ImageJ software (version 1.50i), compensating for the tilt. Images were captured at 20 000 \times , 40 000 \times , and 70 000 \times magnifications.

Synchrotron Macroattenuated Total Reflectance Fourier Transform Infrared Microspectroscopy. A surface chemical characterization of the wing surfaces was performed at the Infrared Microspectroscopy (IRM) beamline at the Australian Synchrotron using a Bruker Hyperion 2000 FTIR microscope equipped with a liquid nitrogen-cooled narrow-band mercury cadmium telluride (MCT) detector, coupled to a VERTEX V80v FTIR spectrometer (Bruker Optik GmbH, Ettlingen, Germany).

The spatially resolved distribution of the chemical functional groups present in the dragonfly wings was imaged in a macro-attenuated total reflection–Fourier transform infrared (ATR–FTIR) mapping mode, as previously described.²⁷ An in-house developed macro-ATR–FTIR device equipped with a 100 μm diameter facet germanium (Ge) ATR crystal ($n_{\text{Ge}} = 4.0$) and a 20 \times IR objective (NA = 0.60; Bruker Optik GmbH, Ettlingen, Germany) was used. The unique combination of the high refractive index of the Ge ATR crystal and the high NA objective used in this device, when coupled to the synchrotron-IR beam, allowed the surface characterization of the wing samples to be performed at a high spatial resolution down to approximately 1 μm .

The wing section was mounted on an aluminum disc using a polyimide (Kapton) tape to hold both sides of the wing. The aluminum disc was then placed into the sample stage of the macro-ATR–FTIR unit. Subsequently, the Ge ATR crystal was brought to the focus of the synchrotron-IR beam, and a background spectrum was recorded in air using 4 cm^{-1} spectral resolution and 128 co-added scans. The wing sample was then brought into contact with the sensing facet of the Ge ATR crystal, and a synchrotron macro-ATR–FTIR chemical map was acquired to cover an area of $40\text{ }\mu\text{m} \times 40\text{ }\mu\text{m}$ within the wing membrane. Every spectrum was collected with a beam defining aperture providing a nominal measurement area of 3.1 μm diameter per pixel, at 1 μm step intervals. For each pixel, the synchrotron macro-ATR–FTIR spectrum was recorded within a spectral range of 3800–700 cm^{-1} using 4 cm^{-1} spectral resolution and 16 co-added scans. Blackman-Harris 3-Term apodization, power-spectrum phase correction, and a zero-filling factor of 2 were set as the default acquisition parameters using the OPUS 7.2 software suite (Bruker), which was also used for data analysis. Chemical maps were generated from the embedded spectra by integrating the area under the relevant peaks. In particular, the distributions of lipid and protein were analyzed by integrating the area under the ester carbonyl stretching band (1720–1750 cm^{-1}) and amide I band (1600–1705

cm^{-1}), respectively. The ratio of lipid to protein was also generated using OPUS 7.2 software.

Water Contact Angle Measurements. Surface wettability was examined by measurement of the static water contact angles (WCAs) using the sessile drop method. The static contact angle was taken as the point prior to droplet elongation as the tip was drawn away from the surface. All measurements were carried out in air using an FTA1000c instrument equipped with a nanodispenser (First Ten Ångströms, Inc., Portsmouth, VA). Measurements were taken across the entire surfaces of the natural and gold-coated dragonfly forewings.

Preparation of Vesicles. GUVs were prepared following a method that was adapted from that described by Weinberger et al.¹⁹ Glass slides were cleaned with chloroform, acetone, and 100% ethanol and dried with N_2 gas between each step prior to being UV ozone cleaned for 1 h. Polyvinyl alcohol (PVA) gels (MW 13–23 kDa) were prepared at concentration 5% w/v in Milli-Q water. Aliquots (100–150 μL) of the PVA solution were spread on the glass slides and dried in an oven at 80 °C for 30 min until a thin film was formed. DOPC (20–30 μL ; 1 mg/mL), with 1 mol % fluorescently labeled Liss Rhod PE, solutions in chloroform were deposited onto the dry PVA surface. The chloroform from the DOPC solution was allowed to fully evaporate under vacuum to form lipid stacks. Grace Bio-Labs CoverWell (Bend, OR) rubber perfusion chambers (9 × 2.5 mm diameter × thickness) were cleaned using the same procedure used for the glass slides and placed over the dried lipid stacks to create a well. A portion of 130 μL of the swelling solution (0.9% w/v NaCl plus 2% w/v FITC–dextran) was added to the wells and allowed to equilibrate for 20 min, allowing encapsulation of dextran to take place. The resultant swollen vesicles were then transferred to an Eppendorf tube and excess 0.9% NaCl was added, creating an osmotic pressure difference inside and outside of the GUVs. The GUVs were allowed to settle over a period of at least 2 h before being gently washed in 0.9% NaCl. This washing step was repeated twice to remove the majority of excess dextran in solution. GUVs were stored in the 0.9% NaCl bulk solution at 5 °C until needed.

Confocal Laser Scanning Microscopy. Natural and gold-coated dragonfly wing sections were taped to microscope cover glasses (Marienfeld Superior, Lauda-Königshofen, Germany) and surrounded by a waterproof silicone gel (Monarch Painting, Victoria, Australia) to create a well approximately 5 mm in height and left to dry overnight. Gold coating of the wing samples, for the analysis of GUV–surface interactions, was performed using a JEOL NeoCoater (JEOL Inc., Peabody, MA), generating thin gold films on the surface of ~ 4.5 nm thickness according to the manufacturers' instructions. GUV (100 μL) solution was then added to the wing surface and allowed to equilibrate for 6 h. Confocal laser scanning microscopy (CLSM) was used to visualize the interaction between the GUVs and the nanostructures present on the wing surfaces. Liss Rhod PE fluoresces red and FITC–dextran fluoresces green upon laser excitation at wavelengths of 560 and 492 nm, respectively. Imaging was performed at 600× magnification using a FluoView FV1000 inverted microscope (Olympus, Tokyo, Japan). z-Stack images were analyzed using Fiji ImageJ to enable 3D reconstructions of the adsorbed GUVs.

Cryo-Scanning Electron Microscopy. Prior to the cryo-scanning electron microscopy (cryo-SEM) imaging, insect wings were attached to an SEM copper stage using a Tissue-Tek glue (Sakura Finetek, Alphen aan den Rijn, The Netherlands). GUV suspension (50 μL) was then applied on the top of the wings and was left for half an hour to allow the GUVs to settle onto the wing surfaces. The samples with GUVs were then manually plunge frozen into liquid N_2 and transferred into the cryo stage prechamber, Alto 2500 (Gatan, UK) at -140 °C, before being sublimed at -95 °C for 20 min to remove free water molecules. Samples were then coated with 5 nm Au/Pd at -140 °C. After Au/Pd coatings, samples were transferred into the SEM stage at -140 °C. Samples were then imaged using FEI Quanta 200F SEM (Thermo Fischer Scientific, Hillsboro, OR) at 10 kV.

Statistical Analysis. SPSS version 25 (IBM Corp., Armonk, NY) was used to test the height and diameter of free-standing nanopillars and the nanofeature density for normality with Shapiro–Wilk tests.

Levene's test was used to check for homogeneity of variance before performing independent t -tests with a significance threshold set at $p = 0.05$. The natural imperfections and variation on the surface of the dragonfly wings meant that the height and diameter of the free-standing nanopillars had to be measured manually, and hence a limited number of measurements were taken.

RESULTS AND DISCUSSION

Surface Characteristics of Dragonfly Wings. Analysis of top-view and tilted SEM images revealed an irregular pattern of nanopillars on the wing epicuticle layer of both species of dragonflies (Figures 1 and S1). The unique nanostructure of

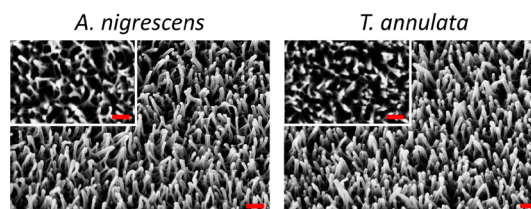


Figure 1. Surface nanoarchitecture of *A. nigrescens* and *T. annulata* dragonfly wing membranes. Typical tilted and top-view (inset) SEM images showing the characteristic irregular nanopillar pattern on the wing epicuticle of both dragonfly species. Scale bars are 200 nm.

the wings of the two studied species of dragonflies was found to be consistent with that of previously studied species.^{1,2} It appeared that the characteristic nanostructure of the wings is highly conserved across dragonflies from different families and geographic locations.^{1–4,28}

The nanopillar dimensions were found to be similar for both dragonfly wing samples, with the average height ranging from 307 ± 34 nm for *A. nigrescens* and 292 ± 34 nm for *T. annulata* ($p = 0.201$) and average diameter of free-standing nanopillars ranging from 45 ± 7 nm for *A. nigrescens* and 42 ± 6 nm for *T. annulata* ($p = 0.133$). The similarity in pillar heights and diameters is remarkable considering the differences in geographic location, habitat preference, and migratory behavior between the two species (Table 1). However, the density of nanofeatures, as measured by particle analysis from top-view SEM images, including free-standing and clustering nanopillars, was found to be different ($p < 0.001$) between the two studied species (Table 1 and Figure 1). The nanofeature density observed for the European *T. annulata* wing was significantly higher than that presented on the Australian *A. nigrescens* wing. Gold coating of the wing surfaces resulted in thin gold films on the surface of 4.5 nm thickness, which was not expected to significantly disrupt the unique nanoarchitecture (as previously shown for similar nanoscale features on the surface of the wings of cicadas).²⁹ Cross-sectional scanning electron micrographs demonstrated similar nanopillar arrays present on wing surface samples in their natural state compared to those coated with gold prior to freeze fracturing (Figure S2).

The chemical composition of the wing membrane for each dragonfly was determined using synchrotron-sourced macro-ATR–FTIR microspectroscopy, generating high-resolution spatial mapping of the epicuticular surface and underlying cuticle layer, which primarily consists of protein and chitin (Figure 2).^{1,32}

The average spectra from each wing sample, as shown in Figure 2a, appeared to be broadly similar. The spectral features in the high wavenumber region (i.e., 3500–2800 cm^{-1})

Table 1. Lifestyle and Wing Surface Characteristics of Two Dragonfly Species

species	geographic location	migratory	preferred habitat	nanopillar height (nm)	diameter of free-standing nanopillars (nm)	nanofeature density ^a (per μm^2)
<i>A. nigrescens</i>	Australia	no	still water ³⁰	307 \pm 34	45 \pm 7	47 \pm 3
<i>T. annulata</i>	Europe	yes	still and running water ³¹	292 \pm 34	42 \pm 6	60 \pm 3

^aNanofeature density includes both free-standing and clustering nanopillars.

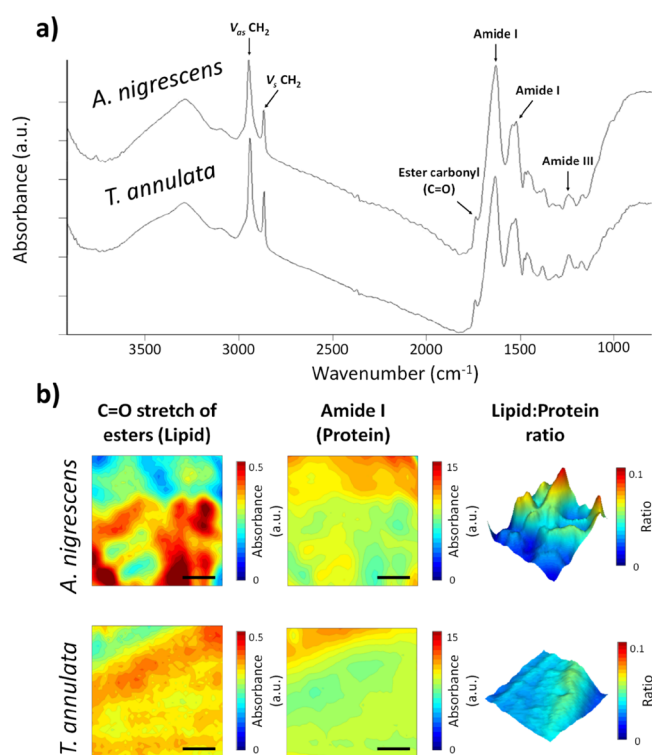


Figure 2. Chemical composition and distribution of the wing membrane surface of two dragonflies, *A. nigrescens* and *T. annulata*, acquired using synchrotron macro-ATR-FTIR microspectroscopy. (a) Average synchrotron macro-ATR-FTIR spectra of the two wing samples. (b) 2D chemical maps of lipid and protein presented on the wing membranes and the corresponding 3D contour maps of the lipid to protein ratio (shown from left to right). Scale bars are 10 μm .

contain (i) broad overlapping bands of O–H stretching modes within the range 3500–3200 cm^{-1} and (ii) characteristic bands of the C–H stretching vibrations of both lipids and proteins. The other prominent peak relevant to the lipid moiety occurs in the lower wavenumber region at $\sim 1740 \text{ cm}^{-1}$ assignable to C=O stretches of ester functional groups from lipid triglycerides and fatty acids and is therefore commonly used to represent total lipids in the analyzed material.^{33–36} The bands at 1650, 1535, and 1240 cm^{-1} are attributed to amide I, II, and III modes in proteins, respectively. In principle, amide I and amide II bands arise due to C=O stretching coupled to N–H bending modes and C–N stretching coupled to N–H bending modes, respectively.³⁵ Among these spectral regions, amide I band has been found to be the most sensitive to the variations in secondary structure folding of peptides and proteins and commonly used as a representative of protein components in the material. In most insect wings, the presence of amide groups can be attributed to chitin and protein, which are the major structural components of the insect cuticle.³⁷

In addition, the chemical maps of the dragonfly wings in Figure 2b revealed spatial variations of lipid and protein

distributions on the wing membrane, according to the integrated areas under the ester carbonyl (1750–1720 cm^{-1}) and amide I (1705–1600 cm^{-1}) peaks, respectively. Although the protein distribution across the wing surface was relatively homogeneous for both individuals, the wing of *A. nigrescens* displayed a more heterogeneous distribution of lipids across the wing compared to that of *T. annulata* (Figure 2b).

Surface Wettability of the Dragonfly Wings. Surface wettability was examined by measurement of the static WCAs using the sessile drop method. The static contact angle was measured at the point prior to droplet elongation as the tip was drawn away from the surface. All measurements were carried out in air using an FTA1000c instrument equipped with a nanodispenser. Measurements were taken across the entire surface of each natural and gold-coated dragonfly forewing.

The wettability of the natural and gold-coated wing surfaces of both dragonflies was determined through the measurement of the static WCA. As expected, the surfaces of both dragonfly wings were superhydrophobic, with WCAs of $162 \pm 8^\circ$ for *A. nigrescens* and $167 \pm 6^\circ$ for *T. annulata*. Each contact angle is above the accepted threshold for superhydrophobicity ($>150^\circ$) (Figure 3). The superhydrophobicity of the surfaces results

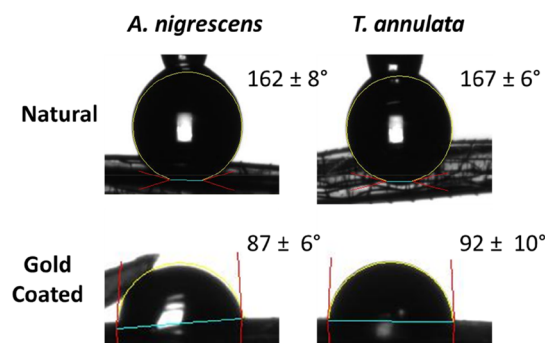


Figure 3. WCAs of *A. nigrescens* and *T. annulata* wings in their natural state (top) and coated with a thin film of gold (bottom).

from the unique physico-chemical make-up of the wing nanostructure and lipid composition, which affords both anti-wetting and anti-biofouling properties to the wings.^{32,38} The ability to efficiently expel water from the wing surface acts as a self-cleaning mechanism, removing potential biological and non-biological contaminants. Such contaminants would otherwise weigh down the ultralight wings, adversely affecting the finely tuned aerodynamic properties that are critical for successful flight and survival of dragonflies.^{39,40}

When coated with a thin film of gold, the surface of the *A. nigrescens* and *T. annulata* wings exhibited static WCAs of $87 \pm 6^\circ$ and $92 \pm 10^\circ$, respectively (Figure 3). The reduction in WCA is due to the change in surface chemistry when the wings were coated with the more hydrophilic gold atoms.^{3,29} This 4.5 nm thick coating did not significantly affect the unique nanoarchitecture of the wings (Figure S2). The static WCA of

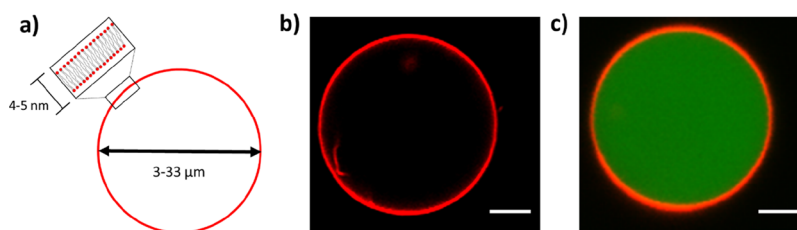


Figure 4. GUVs. (a) Schematic illustration of a GUV. CLSM images of GUVs with Liss Rhod B labeled DOPC membranes (colored in red) with two types of swelling solutions: (b) 0.9% NaCl and (c) 0.9% NaCl and 2% FITC–dextran (colored in green). Scale bars are 10 μm .

the nanostructured surfaces was found to be greater than that measured on smooth gold surfaces, which is likely due to the pockets of entrapped air between the nanopillars, which is in agreement with the Cassie–Baxter model for non-wetting behaviors of nanostructured surfaces.⁴¹

Phospholipid Membrane Model. The GUVs were prepared using the PVA-assisted gentle swelling method, as developed by Weinberger et al., for use as a simplified model of the phospholipid membrane.¹⁹ The GUVs prepared were in the size range of 3–33 μm in diameter, with over 70% of GUVs being between 5 and 20 μm in diameter (Figures 4 and S3).

Controlling the concentration of solutes in the swelling solution (inside) and bulk solution (outside) allows the internal osmotic pressure (Π) of the GUVs to be calculated from the internal concentration of the solute (M), the ideal gas constant (R), and the absolute temperature (T), as described by $\Pi = MRT$.⁴² In this study, the GUVs were swelled with 2% FITC–dextran (1.3×10^{-4} M) at room temperature (298.15 K), with the ideal gas constant assumed to be 8.314 L kPa mol⁻¹ K⁻¹. The internal osmotic pressure was calculated to be 0.33 kPa which is equivalent to 330 N m⁻².

Because of the outward pressure being exerted, the subsequent increase in the internal osmotic pressure increases the isotropic tension, or degree of stretching, experienced by the vesicle membrane increasing the rigidity and likelihood of rupture.⁴³ The isotropic tension (\bar{T}) can be defined as a function of the difference between the internal and external osmotic pressure (P) and the vesicle radius (R_0), as described $\bar{T} = PR_0/2$.⁴⁴ The radius of the fabricated GUVs ranged from 1.5 to 16.5 μm , with 5–15 μm in diameter of the majority of GUVs (Figure S3). Using $P = 330$ N m⁻² (as calculated above), we find that \bar{T} ranges from 0.25–2.7 mN m⁻¹.

The biophysical properties of the membrane are related to its chemical composition.⁴⁵ Micropipette aspiration is typically used to determine the tensile rupture limit of GUVs; however, factors such as the applied loading rate result in variable outcomes. For example, Jalmar et al. used the measurements of the elastic modulus of the membrane to quantify the tensile rupture limit of GUVs composed of DOPC and found it to be 12 ± 1 mN m⁻¹.⁴⁶ Contrastingly, under constant tension conditions, Levadny et al. reported the rupture of an entire population of GUVs, which occurred at 7 mN m⁻¹.⁴⁷ In the case of the nanostructured, bactericidal surfaces, the membrane tensions imposed on the GUVs from the surface are relatively constant and hence the latter value is more relevant as an estimation of the maximum tensile rupture limit. This can be taken as the maximum limit of tensile force or the degree of stretching; the vesicle membrane is able to withstand before rupturing. By determining the difference in the isotropic tension generated by the internal osmotic pressure and the maximum tensile rupture limit of the DOPC GUV, the

minimum amount of additional tension required to mechanically rupture the GUVs can be determined as 4.3–6.8 mN m⁻¹, dependent on the relative size of the GUV. Hence, the deformation of GUVs inducing a loss of integrity or membrane pore formation, on the nanostructured wing surfaces, indicates the presence of tensions being exerted that are in excess of 6.8 mN m⁻¹.

Interactions of GUVs with Nanostructured Dragonfly Wing Surfaces. The interactions between bacterial cells and surfaces with high-aspect-ratio nanoscale features have been previously well investigated over a range of materials.^{2–6,29} However, there are comparatively fewer studies of unilamellar vesicles on such surfaces, with research focusing on nanopores and nanoparticles, which are often chemically functionalized.^{48–50} Analysis of CLSM z-stack images indicated that the GUVs of approximately 10 μm in diameter were able to adsorb on the natural and gold-coated wing surfaces of both dragonfly species; however, the typical spherical morphology of the vesicles appeared significantly altered (Figures 5 and

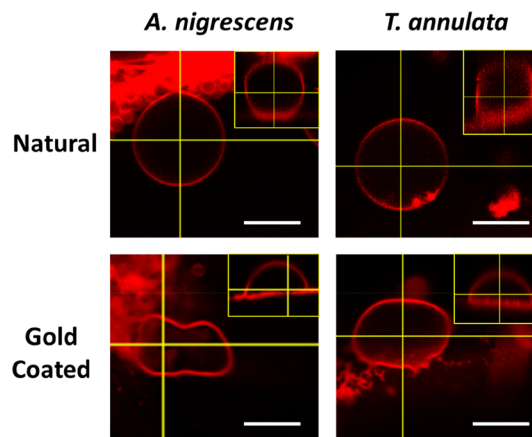


Figure 5. CLSM images of GUV interactions with the surface of natural and gold-coated *A. nigrescens* and *T. annulata* wings. Large images represent top view. Insets are generated through confocal z-stacks using Fiji ImageJ software and demonstrate the cross section of the GUV deforming on the nanostructured surfaces. Scale bars are 10 μm .

S4). Using gold-coated *T. annulata* wing surfaces, it is also confirmed that the membrane tension plays a role in GUV interactions with wing surfaces: the morphology of the GUVs fabricated with 3% dextran appeared to be altered to a greater degree in comparison to GUVs fabricated with 1% dextran (Figure S5).

Despite differences in the nanofeature density present on the wing surface of the two dragonflies, there was no observable difference in the deformation behavior of the GUVs between the two species. The mechano-bactericidal mechanism is

thought to be highly conserved across species because of the important evolutionary advantages; however, previous work demonstrated differences present in the bactericidal efficiency of wing surfaces from different species.² Greater deformation was observed on the gold-coated wing surfaces (Figure 5), which may be due to the increased surface–vesicle interactions with the gold, which is more hydrophilic than the natural waxy wing epicuticle (Figure 3). Such a decrease in hydrophobicity would increase the interaction affinity taking place between the surface and the GUVs, which are covered in hydrophilic phospholipid heads, surrounded by a thin hydration layer.⁵¹ The leakage of FITC–dextran out of GUVs was observed for GUVs interacting with native and gold-coated wing surfaces (Figures S6 and S7). The interactions of GUVs with gold-coated *T. annulata* wing surfaces were determined in a dynamic study based on real-time sequential confocal imaging (Figure S7), which provided an insight into the initial damage to the GUV membrane. It was found that the leakage of FITC–dextran out of GUVs can be detected at the 1 and 2 h timepoints, with the size of the GUV significantly reduced with the progressive leakage of dextran (Figure S7).

To further investigate the observed deformation of the GUVs upon interacting with the surfaces, cryo-SEM was utilized. Cryo-SEM allows extremely high-resolution imaging of the behavior of GUVs upon interacting with the wing surfaces in their natural hydrated state, unachievable through conventional SEM. The solution, containing GUVs, was applied on the wing surfaces and left for half an hour to allow the majority of GUVs to settle, before being plunge frozen in liquid N₂. Free water molecules were removed by sublimation for 20 min at –95 °C before the GUVs were cryogenically gold-coated and imaged (Figure 6).

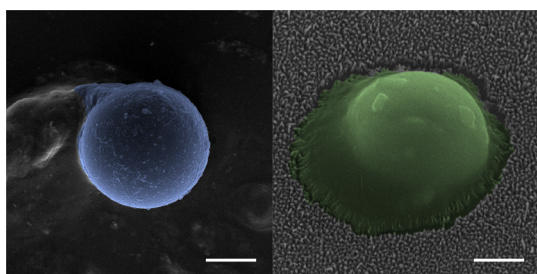


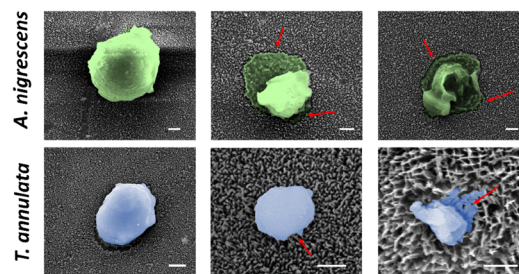
Figure 6. Cryo-scanning electron micrographs showing a spherical GUV remaining intact (left) in solution and deformed truncated sphere-like GUV (right) upon interacting with the nanostructured natural wing surface of *T. annulata*. Scale bars are 1 μm .

Cryo-scanning electron micrographs demonstrate that the GUV membrane adsorbs on the surface, then deforms, to partially envelop the nanopillars (Figure 6). The membrane appears to stretch at the GUV–surface interface, extending beyond the radius of the vesicle when intact and spherical. In this case, the deformed vesicle appears to be stretched with a truncated sphere-like shape which is consistent with the CLSM images (Figure 5). This suggests that the membrane is being distributed across the surface, whereas the truncated sphere-like shape possesses an increased surface area/volume ratio, in comparison to the spherical GUV in solution. The stretching of the membrane is equivalent to the stretching of the bacterial cell wall on similar nanostructured surfaces.^{2,3}

High-resolution cryo-scanning electron micrographs provide evidence of different degrees of deformation of the GUV

membrane, as well as its apparent rupture, most likely because of different durations of the interactions (Figure 7). This

Natural



Gold Coated

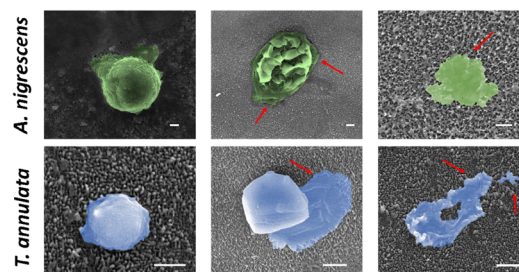


Figure 7. Cryo-scanning electron micrographs demonstrating the interactions between the GUVs and the nanostructured natural wing surface (top) and gold-coated wing surface (bottom) of *A. nigrescens* and *T. annulata*. Different stages of rupture, including intact GUVs (left), deformation (middle), and apparent rupture (right) can be visualized because of the different times taken for individual GUVs to settle on the surface. Red arrows indicate membrane deformation on the nanostructured surfaces. Scale bars are 1 μm .

suggests that the process of deformation is gradual. This is possibly due to the flexibility of the DOPC membrane, when compared to the bacterial cell wall, which tolerates greater curvature around the nanopillars present on the dragonfly wing surface. In comparison, the bacterial cell wall is more complex and rigid, consisting of different types of phospholipids, membrane-bound proteins, layers of peptidoglycan and is often connected to an internal cytoskeleton, which decreases the membrane's flexibility.^{12,52} Additionally, the internal pressure, from osmotic differences across the membrane, may be reduced from the formation of pores which can temporarily open and reseal, allowing the GUV to remain intact.⁵³ It has previously been estimated that bacterial cells can be ruptured on nanostructured surfaces within 3–5 min.²⁹ Nevertheless, eventual rupture of the GUVs composed of DOPC, across a range of sizes, indicates membrane tensions generated from all of the nanostructured surfaces used in this study to be in excess of 6.8 mN m⁻¹, as previously calculated.

Current explanations for individual GUV–surface interactions explain rupture as a result of pore formation because of a strain on the membrane.⁵⁴ Another theoretical study suggests that pore formation likely occurs at the rim of the vesicle–surface contact, as a combination of membrane bending and tension, which is supported by the previous experimental evidence.^{55,56} However, this model focuses on flat surfaces, not taking into account topographically nanostructured surfaces. The membrane deformation at the GUV–surface interface suggests stretching of the phospholipids over the nanoscale features. This is the source of tension imposed on the GUV,

resulting in the formation of pores and in some cases eventual rupture. Interestingly, the membrane interacting with the nanostructured surface appears to extend beyond the circumference of the vesicle (Figure 6). These findings compliment the current model of the mechano-bactericidal mechanism exhibited by nanostructured surfaces.¹¹

CONCLUSIONS

We have presented a simplified model of the bacterial cell membrane through the construction of GUVs, composed of DOPC, to characterize the interactions between the membrane and the nanostructured surface of the wings of two dragonflies. The unique nanoarchitecture present on the dragonflies, both in their natural state and when covered in a thin-film of gold, was able to rupture the GUV model membrane presented here. On the basis of previously reported experimental data pertaining to the membrane rupture of GUVs, composed of DOPC, we can estimate the tensions involved in the interaction between the membrane and the surface nanostructures of the dragonfly wings studied to be above 6.8 mN m^{-1} . To our knowledge, this is the first experimental investigation of the range of forces imparted by mechano-bactericidal nanoarchitectures through a bottom-up approach.

Furthermore, high-resolution cryo-SEM imaging was able to give unique insights into the morphology of GUVs interacting with the nanostructured wing surfaces. The GUVs were observed to deform over the surface nanopillars. The images indicated that the GUVs are capable of sustaining significant deformation before eventually rupturing. As discussed in the previous work, GUVs can form small pores, without exhibiting rupture, to relieve internal osmotic pressure and it is likely that this, at least in combination with other factors, is an explanation for the GUVs remaining intact during such deformation. Hence, the calculated value of 6.8 mN m^{-1} may be a conservative estimate of the tensions generated from the nanostructured surface, as it is possible nano-sized pores form and reseal below this tension.

The simple membrane model employed here offers a novel approach for characterizing the mechano-bactericidal potential of nanostructured surfaces. Future developments of this membrane model, such as altering the phospholipid composition, osmotic pressure, or the addition of other molecules or peptidoglycan layers, could provide additional valuable information. This well-controlled system could be useful in the design optimization for future synthetic nanostructured materials to generate bactericidal activity, such as industrial and biomedical materials, where bacterial colonization is a significant problem.

ASSOCIATED CONTENT

Supporting Information

The Supporting Information is available free of charge on the ACS Publications website at DOI: 10.1021/acs.langmuir.8b03470.

Reconstructed visualization of the wing surface nanostructures, cross-sectional SEM of the natural and gold-coated dragonfly wings, size distribution of GUVs, and additional confocal images of GUV interactions with wing surfaces (PDF)

AUTHOR INFORMATION

Corresponding Author

*E-mail: elena.ivanova@rmit.edu.au.

ORCID

Samuel Cheeseman: 0000-0003-2103-2995

Fabrice Thalmann: 0000-0002-9630-1128

Carlos M. Marques: 0000-0002-3952-0498

Vladimir A. Baulin: 0000-0003-2086-4271

Elena P. Ivanova: 0000-0002-5509-8071

Notes

The authors declare no competing financial interest.

ACKNOWLEDGMENTS

Funding from the Australian Research Council Industrial Transformation Research Hubs Scheme (project number IH130100017) is gratefully acknowledged. The development of the macro-ATR-FTIR device used in this study was part of the Science Projects at Australian Synchrotron initiative that has been made available for the IRM Beamline users. This research was undertaken on the IRM beamline at Australian Synchrotron (Victoria, Australia). We would like to thank the staff from the Bio21 Advanced Microscopy Facility (the University of Melbourne).

REFERENCES

- (1) Ivanova, E. P.; Nguyen, S. H.; Webb, H. K.; Hasan, J.; Truong, V. K.; Lamb, R. N.; Duan, X.; Tobin, M. J.; Mahon, P. J.; Crawford, R. J. Molecular Organization of the Nanoscale Surface Structures of the Dragonfly *Hemianax papuensis* Wing Epicuticle. *PLoS One* **2013**, *8*, No. e67893.
- (2) Mainwaring, D. E.; Nguyen, S. H.; Webb, H.; Jakubov, T.; Tobin, M.; Lamb, R. N.; Wu, A. H.-F.; Marchant, R.; Crawford, R. J.; Ivanova, E. P. The Nature of Inherent Bactericidal Activity: Insights from the Nanotopology of Three Species of Dragonfly. *Nanoscale* **2016**, *8*, 6527–6534.
- (3) Ivanova, E. P.; Hasan, J.; Webb, H. K.; Gervinskas, G.; Juodkazis, S.; Truong, V. K.; Wu, A. H.; Lamb, R. N.; Baulin, V. A.; Watson, G. S. Bactericidal Activity of Black Silicon. *Nat. Commun.* **2013**, *4*, 2838–2844.
- (4) Bandara, C. D.; Singh, S.; Afara, I. O.; Wolff, A.; Tesfamichael, T.; Ostrikov, K.; Oloyede, A. Bactericidal Effects of Natural Nanotopography of Dragonfly Wing on *Escherichia coli*. *ACS Appl. Mater. Interfaces* **2017**, *9*, 6746–6760.
- (5) Bhadra, C. M.; Truong, V. K.; Pham, V. T.; Al Kobaisi, M.; Seniutinas, G.; Wang, J. Y.; Juodkazis, S.; Crawford, R. J.; Ivanova, E. P. Antibacterial Titanium Nano-Patterned Arrays Inspired by Dragonfly Wings. *Sci. Rep.* **2015**, *5*, 16817.
- (6) Linklater, D. P.; Nguyen, H. K. D.; Bhadra, C. M.; Juodkazis, S.; Ivanova, E. P. Influence of Nanoscale Topology on Bactericidal Efficiency of Black Silicon Surfaces. *Nanotechnology* **2017**, *28*, 245301.
- (7) Hasan, J.; Raj, S.; Yadav, L.; Chatterjee, K. Engineering a nanostructured “super surface” with superhydrophobic and super-killing properties. *RSC Adv.* **2015**, *5*, 44953–44959.
- (8) Costerton, J. W.; Montanaro, L.; Arciola, C. R. Biofilm in Implant Infections: Its Production and Regulation. *Int. J. Artif. Organs* **2005**, *28*, 1062–1068.
- (9) Schierholz, J. M.; Beuth, J. Implant Infections: A Haven for Opportunistic Bacteria. *J. Hosp. Infect.* **2001**, *49*, 87–93.
- (10) Wolcott, R. D.; Rhoads, D. D.; Bennett, M. E.; Wolcott, B. M.; Gogokhia, L.; Costerton, J. W.; Dowd, S. E. Chronic Wounds and the Medical Biofilm Paradigm. *J. Wound Care* **2010**, *19*, 45–53.
- (11) Pogodin, S.; Hasan, J.; Baulin, V. A.; Webb, H. K.; Truong, V. K.; Phong Nguyen, T. H.; Boshkovikj, V.; Fluke, C. J.; Watson, G. S.; Watson, J. A.; Crawford, R. J.; Ivanova, E. P. Biophysical Model of

Bacterial Cell Interactions with Nanopatterned Cicada Wing Surfaces. *Biophys. J.* **2013**, *104*, 835–840.

(12) Silhavy, T. J.; Kahne, D.; Walker, S. The Bacterial Cell Envelope. *Cold Spring Harbor Perspect. Biol.* **2010**, *2*, a000414.

(13) Katsikogianni, M.; Missirlis, Y. F. Concise review of mechanisms of bacterial adhesion to biomaterials and of techniques used in estimating bacteria-material interactions. *eCM* **2004**, *8*, 37–57.

(14) Bagatolli, L. A.; Needham, D. Quantitative Optical Microscopy and Micromanipulation Studies on the Lipid Bilayer Membranes of Giant Unilamellar Vesicles. *Chem. Phys. Lipids* **2014**, *181*, 99–120.

(15) Brüggemann, D.; Frohnmayer, J. P.; Spatz, J. P. Model Systems for Studying Cell Adhesion and Biomimetic Actin Networks. *Beilstein J. Nanotechnol.* **2014**, *5*, 1193–1202.

(16) Fenz, S. F.; Sengupta, K. Giant Vesicles as Cell Models. *Integr. Biol.* **2012**, *4*, 982–995.

(17) Stein, H.; Spindler, S.; Bonakdar, N.; Wang, C.; Sandoghdar, V. Production of isolated giant unilamellar vesicles under high salt concentrations. *Front. Membr. Physiol. Membr. Biophys.* **2017**, *8*, 63.

(18) Walde, P.; Cosentino, K.; Engel, H.; Stano, P. Giant Vesicles: Preparations and Applications. *ChemBioChem* **2010**, *11*, 848–865.

(19) Weinberger, A.; Tsai, F.-C.; Koenderink, G. H.; Schmidt, T. F.; Itri, R.; Meier, W.; Schmatko, T.; Schröder, A.; Marques, C. Gel-Assisted Formation of Giant Unilamellar Vesicles. *Biophys. J.* **2013**, *105*, 154–164.

(20) Aimon, S.; Manzi, J.; Schmidt, D.; Larrosa, J. A. P.; Bassereau, P.; Toombes, G. E. S. Functional Reconstitution of a Voltage-Gated Potassium Channel in Giant Unilamellar Vesicles. *PLoS One* **2011**, *6*, No. e25529.

(21) Allen, T. M.; Cullis, P. R. Liposomal Drug Delivery Systems: From Concept to Clinical Applications. *Adv. Drug Delivery Rev.* **2013**, *65*, 36–48.

(22) Gregoriadis, G. Drug Entrapment in Liposomes. *FEBS Lett.* **1973**, *36*, 292–296.

(23) Gracià, R. S.; Bezlyepkina, N.; Knorr, R. L.; Lipowsky, R.; Dimova, R. Effect of Cholesterol on the Rigidity of Saturated and Unsaturated Membranes: Fluctuation and Electrodeformation Analysis of Giant Vesicles. *Soft Matter* **2010**, *6*, 1472–1482.

(24) Sachse, R.; Dondapati, S. K.; Fenz, S. F.; Schmidt, T.; Kubick, S. Membrane protein synthesis in cell-free systems: From bio-mimetic systems to bio-membranes. *FEBS Lett.* **2014**, *588*, 2774–2781.

(25) Zhou, H.; Gabilondo, B. B.; Losert, W.; van de Water, W. Stretching and Relaxation of Vesicles. *Phys. Rev. E: Stat., Nonlinear, Soft Matter Phys.* **2011**, *83*, 011905.

(26) Meister, A.; Finger, S.; Hause, G.; Blume, A. Morphological Changes of Bacterial Model Membrane Vesicles. *Eur. J. Lipid Sci. Technol.* **2014**, *116*, 1228–1233.

(27) Vongsvivut, J.; Truong, V. K.; Al Kobaisi, M.; Maclaughlin, S.; Tobin, M. J.; Crawford, R. J.; Ivanova, E. P. Synchrotron Macro ATR-FTIR Microspectroscopic Analysis of Silica Nanoparticle-Embedded Polyester Coated Steel Surfaces Subjected to Prolonged UV and Humidity Exposure. *PLoS One* **2017**, *12*, No. e0188345.

(28) Nguyen, S. H.; Webb, H. K.; Hasan, J.; Tobin, M. J.; Mainwaring, D. E.; Mahon, P. J.; Marchant, R.; Crawford, R. J.; Ivanova, E. P. Wing Wettability of Odonata Species as a Function of Quantity of Epicuticular Waxes. *Vib. Spectrosc.* **2014**, *75*, 173–177.

(29) Ivanova, E. P.; Hasan, J.; Webb, H. K.; Truong, V. K.; Watson, G. S.; Watson, J. A.; Baulin, V. A.; Pogodin, S.; Wang, J. Y.; Tobin, M. J.; Löbbe, C.; Crawford, R. J. Natural Bactericidal Surfaces: Mechanical Rupture of *Pseudomonas aeruginosa* Cells by Cicada Wings. *Small* **2012**, *8*, 2489–2494.

(30) Theischinger, G.; Hawking, J. *The Complete Field Guide to Dragonflies of Australia*; CSIRO Publishing, 2006.

(31) Boudot, J.-P.; Clausnitzer, V.; Ferreira, S.; Suhling, F.; Dijkstra, K.-D. B.; Schneider, W.; Samraoui, B. *Trithemis annulata*. *The IUCN Red List of Threatened Species*; IUCN, 2016.

(32) Nguyen, S. H. T.; Webb, H. K.; Hasan, J.; Tobin, M. J.; Crawford, R. J.; Ivanova, E. P. Dual Role of Outer Epicuticular Lipids

in Determining the Wettability of Dragonfly Wings. *Colloids Surf., B* **2013**, *106*, 126–134.

(33) Coury, C.; Dillner, A. M. A Method to Quantify Organic Functional Groups and Inorganic Compounds in Ambient Aerosols using Attenuated Total Reflectance FTIR Spectroscopy and Multivariate Chemometric Techniques. *Atmos. Environ.* **2008**, *42*, 5923–5932.

(34) Lasch, P.; Boese, M.; Pacifico, A.; Diem, M. FT-IR Spectroscopic Investigations of Single Cells on the Subcellular Level. *Vib. Spectrosc.* **2002**, *28*, 147–157.

(35) Barth, A. Infrared Spectroscopy of Proteins. *Biochim. Biophys. Acta, Bioenerg.* **2007**, *1767*, 1073–1101.

(36) Vongsvivut, J.; Heraud, P.; Gupta, A.; Puri, M.; McNaughton, D.; Barrow, C. J. FTIR Microspectroscopy for Rapid Screening and Monitoring of Polyunsaturated Fatty Acid Production in Commercially Valuable Marine Yeasts and Protists. *Analyst* **2013**, *138*, 6016–6031.

(37) Vincent, J. F. V.; Wegst, U. G. K. Design and Mechanical Properties of Insect Cuticle. *Arthropod Struct. Dev.* **2004**, *33*, 187–199.

(38) Wan, Y.-l.; Cong, Q.; Wang, X.-j.; Yan, Z. The Wettability and Mechanism of Geometric Non-Smooth Structure of Dragonfly Wing Surface. *J. Bionic Eng.* **2008**, *5*, 40–45.

(39) Wagner, T.; Neinhuis, C.; Barthlott, W. Wettability and Contaminability of Insect Wings as a Function of their Surface Sculptures. *Acta Zool.* **1996**, *77*, 213–225.

(40) Nguyen, S.; Webb, H.; Mahon, P.; Crawford, R.; Ivanova, E. Natural Insect and Plant Micro-/Nanostructured Surfaces: An Excellent Selection of Valuable Templates with Superhydrophobic and Self-Cleaning Properties. *Molecules* **2014**, *19*, 13614–13630.

(41) Abdelsalam, M. E.; Bartlett, P. N.; Kelf, T.; Baumberg, J. Wetting of Regularly Structured Gold Surfaces. *Langmuir* **2005**, *21*, 1753–1757.

(42) Pukkahuta, C.; Suwannawat, B.; Shobsngob, S.; Varavinit, S. Comparative study of pasting and thermal transition characteristics of osmotic pressure and heat-moisture treated corn starch. *Carbohydr. Polym.* **2008**, *72*, 527–536.

(43) Jackman, J. A.; Choi, J.-H.; Zhdanov, V. P.; Cho, N.-J. Influence of Osmotic Pressure on Adhesion of Lipid Vesicles to Solid Supports. *Langmuir* **2013**, *29*, 11375–11384.

(44) Needham, D.; Hochmuth, R. M. Electro-Mechanical Permeabilization of Lipid Vesicles. Role of Membrane Tension and Compressibility. *Biophys. J.* **1989**, *55*, 1001–1009.

(45) Janmey, P. A.; Kinnunen, P. K. J. Biophysical Properties of Lipids and Dynamic Membranes. *Trends Cell Biol.* **2006**, *16*, 538–546.

(46) Jalmar, O.; François-Moutal, L.; García-Sáez, A.-J.; Perry, M.; Granjon, T.; Gonzalez, F.; Gottlieb, E.; Ayala-Sanmartin, J.; Klösigen, B.; Schwille, P. Caspase-8 Binding to Cardiolipin in Giant Unilamellar Vesicles Provides a Functional Docking Platform for Bid. *PLoS One* **2013**, *8*, No. e55250.

(47) Levadny, V.; Tsuboi, T.-a.; Belaya, M.; Yamazaki, M. Rate Constant of Tension-Induced Pore Formation in Lipid Membranes. *Langmuir* **2013**, *29*, 3848–3852.

(48) Pfeiffer, I.; Petronis, S.; Köper, I.; Kasemo, B.; Zäch, M. Vesicle Adsorption and Phospholipid Bilayer Formation on Topographically and Chemically Nanostructured Surfaces. *J. Phys. Chem. B* **2010**, *114*, 4623–4631.

(49) Kresák, S.; Hianik, T.; Naumann, R. L. C. Giga-Seal Solvent-Free Bilayer Lipid Membranes: From Single Nanopores to Nanopore Arrays. *Soft Matter* **2009**, *5*, 4021–4032.

(50) Zhang, S.; Nelson, A.; Beales, P. A. Freezing or Wrapping: The Role of Particle Size in the Mechanism of Nanoparticle-Biomembrane Interaction. *Langmuir* **2012**, *28*, 12831–12837.

(51) Rand, R. P.; Parsegian, V. A. Hydration Forces between Phospholipid Bilayers. *Biochim. Biophys. Acta, Rev. Biomembr.* **1989**, *988*, 351–376.

- (52) Hayhurst, E. J.; Kailas, L.; Hobbs, J. K.; Foster, S. J. Cell Wall Peptidoglycan Architecture in *Bacillus subtilis*. *Proc. Natl. Acad. Sci. U.S.A.* **2008**, *105*, 14603–14608.
- (53) Sandre, O.; Moreaux, L.; Brochard-Wyart, F. Dynamics of Transient Pores in Stretched Vesicles. *Proc. Natl. Acad. Sci. U.S.A.* **1999**, *96*, 10591–10596.
- (54) Hamai, C.; Cremer, P. S.; Musser, S. M. Single Giant Vesicle Rupture Events Reveal Multiple Mechanisms of Glass-Supported Bilayer Formation. *Biophys. J.* **2007**, *92*, 1988–1999.
- (55) Zhdanov, V. P. Mechanism of Rupture of Single Adsorbed Vesicles. *Chem. Phys. Lett.* **2015**, *641*, 20–22.
- (56) Kataoka-Hamai, C.; Yamazaki, T. Induced Rupture of Vesicles Adsorbed on Glass by Pore Formation at the Surface-Bilayer Interface. *Langmuir* **2015**, *31*, 1312–1319.